Rare Metal Materials and Engineering
Volume 54, Issue 12, December 2025
Available online at www.rmme.ac.cn

Science Press

Cite this article as: Jin Jufeng, Zhao Xinbao, Zhao Qianmin, et al. Microstructure Characteristics and Strengthening Mechanism of Ni-based Wrought Superalloy GH4350: A Review[J]. Rare Metal Materials and Engineering, 2025, 54(12): 3065-3076. DOI: https://doi.org/10.12442/j.issn.1002-185X.20240656.

REVIEW

Microstructure Characteristics and Strengthening Mechanism of Ni-based Wrought Superalloy GH4350: A Review

Jin Jufeng[1,2], Zhao Xinbao[1,3], Zhao Qianmin[1,2], Yue Quanzhao[1], Gu Yuefeng[1,3], Zhang Ze[1,3]

[1] Institute of Superalloys Science and Technology, School of Materials Science and Engineering, Zhejiang University, Hangzhou 310027, China; [2] Polytechnic Institute, Zhejiang University, Hangzhou 310027, China; [3] State Key Laboratory of Silicon and Advanced Semiconductor Materials, Zhejiang University, Hangzhou 310027, China

Abstract: GH4350 (AEREX 350) is a Ni-based wrought superalloy for high-performance fasteners, with a maximum service temperature of 750 °C. It has high tensile strength, fatigue resistance, stress rupture and relaxation resistance, corrosion resistance, low thermal expansion, and notch sensitivity. The high strength of GH4350 is largely derived through solid solution strengthening and the γ' phase precipitation strengthening. During the precipitation of γ' phase, a minor amount of η phase also precipitates. However, it is reported that the microstructure of alloy is sensitive to heat treatment parameters, including temperature and time. The γ' phases can be transformed into η phases under certain conditions, potentially degrading the performance of the alloy. The chemical composition characteristics, heat treatment strategies, and strengthening mechanism of GH4350 were reviewed in this research, aiming to understand the factors behind its remarkable high-temperature performance, to guide the development of new alloys, and to further enhance its heat resistance.

Key words: wrought superalloy GH4350 for fasteners; high-temperature property; chemical composition; heat treatment; η phase

1 Introduction

Superalloys are extensively used in sectors such as aerospace, energy, and metallurgy due to their capacity to retain superior mechanical properties and structural stability under extreme thermal conditions, where conventional materials will fail due to oxidation, creep, and fatigue[1–4]. Typical superalloys include Ni-based, Co-based, Al-based, Cr-based, and Pt-Al superalloys[2,5–9]. The demands of the modern aerospace industry, particularly for aero engines, require enhanced thrust-to-weight ratios and greater fuel efficiency at elevated temperatures, thereby necessitating the development of increasingly advanced superalloys[1–2].

Ni-based wrought superalloy is a kind of advanced superalloy that exhibits remarkable high-temperature properties including resistance to oxidation, fatigue, and creep. And it is extensively used in diverse industrial sectors, including aerospace, energy, and marine shipping[5–8]. Fasteners, which are used extensively in the aerospace industry, are usually made of Ni-based wrought superalloys. Their primary function is to join multiple separate components into a unit, which makes them an indispensable element in modern industry[10].

GH4350 represents as a Ni-based wrought superalloy used for fasteners due to its ability to withstand service temperatures up to 750 °C[11–13]. Consequently, it must exhibit high tensile and yield strength, along with strong resistance to fatigue, stress rupture, and stress relaxation[14–17]. Additionally, corrosion resistance, low thermal expansion, and low notch sensitivity are critical factors in fastener applications, particularly at elevated temperatures[15,18]. The production of high-quality superalloy ingots is crucial for achieving the remarkable properties required for such demanding applications. Single-melting techniques such as vacuum induction melting (VIM), vacuum arc remelting (VAR), and electro slag remelting (ESR) are used to produce high-quality

Received date: December 10, 2024
Foundation item: Hundred Talents Program of Zhejiang University
Corresponding author: Zhao Xinbao, Ph. D., Professor, Institute of Superalloys Science and Technology, School of Materials Science and Engineering, Zhejiang University, Hangzhou 310027, P. R. China, Tel: 0086-571-64219632, E-mail: superalloys@zju.edu.cn; Gu Yuefeng, Ph. D., Professor, Institute of Superalloys Science and Technology, School of Materials Science and Engineering, Zhejiang University, Hangzhou 310027, P. R. China, Tel: 0086-571-64219632, E-mail: guyf@zju.edu.cn

superalloy ingots with fewer oxides, such as Al_2O_3 particles[2,8]. To further enhance ingot quality, particularly by reducing inclusions, the duplex-melting processes (VIM+VAR and VIM+ESR) and triple-melting processes (VIM+VAR+ESR) are employed in the melting of GH4350 master ingots[8,12,19].

Following alloy smelting, the microstructure is refined through a combination of cold and hot working techniques along with heat treatment, which are designed based on the chemical composition and microstructure characteristics, to further improve the properties of the alloy[19]. Previous research has confirmed that in GH4350, the addition of Co, W, and Mo contributes to solid solution strengthening in the face-centered cubic (fcc) γ phase, while the addition of Al, Ti, Nb, and Ta forms γ' phase, which is distributed throughout the γ phase matrix for precipitation strengthening[12–13,18,20–21]. In addition to the γ' phase, the formation of the hexagonal close-packed (hcp) η phase is notable. This phase forms during heat treatments and is sensitive to temperature and time[21–22]. Understanding the morphology and distribution of η phase is pivotal, as these factors can determine whether its presence is beneficial or detrimental to the properties of alloys[23–27].

The chemical composition of GH4350 and its various heat treatments are reviewed in detail, focusing on different microstructures, such as the distribution of γ' and η phases. It aims to offer valuable insights for optimizing chemical composition and enhancing the existing properties of GH4350 with the goal of further increasing its service temperatures.

2 Chemical Composition and Phase Constitution

2.1 Chemical composition of GH4350

The microstructures of several commonly used Ni-based wrought superalloys for fasteners are summarized in Fig. 1. GH4350, with a service temperature of 750 °C, is derived from the Co-based superalloys MP35N and MP159[12,31]. As illustrated in Fig. 1a, the γ' phases are spherical, with an average diameter of 38 nm, and are uniformly distributed throughout the γ matrix[15]. Additionally, plate-like or needle-like η phases predominantly precipitate at grain boundaries, with a smaller fraction of finer η phases forming within the grains[14–15]. In contrast, alloy 718, as depicted in Fig. 1b–1c, is primarily strengthened by γ'' phases, with a minor presence of spherical γ' phases[14]. Short rod-like δ phases and a small amount of blocky MC carbide are presented on grain boundaries[14]. Alloy 718 Plus, shown in Fig. 1d, is mainly strengthened by γ' phases, accompanied by minor precipitations of η or δ phases[29]. Furthermore, as illustrated in Fig. 1e, Waspaloy exhibits a bimodal distribution of γ' phases, containing spherical primary γ' phases and secondary γ' phases within the matrix, with carbides forming along grain boundaries as a result of heat treatments[14]. A similar distribution of γ' phases is observed in GH4698, as shown in Fig. 1f[30].

These microstructural differences stem from differences in chemical composition, as listed in Table 1. GH4350 contains solid solution strengthening elements like W and Mo, as well as precipitation strengthening elements Al and Ti, leading to the precipitations of γ' phase and η phase. Furthermore, Ta is added into GH4350 to improve its mechanical properties. Some reports demonstrated that the volume fraction of the γ' phase of the alloy aged at 850 °C for 4 h is approximately 18%[13]. Obviously, GH4350 differs from other wrought Ni-based superalloys in elemental composition. Alloy 718 has more Nb and less Al and Ti, which leads to the precipitation of more γ'' phases and less γ' phases[35–38]. The volume fraction of γ'' phase in a wrought alloy 718 (17.8%) is nearly 3 times higher than that of the γ' phase (6.5%). However, at

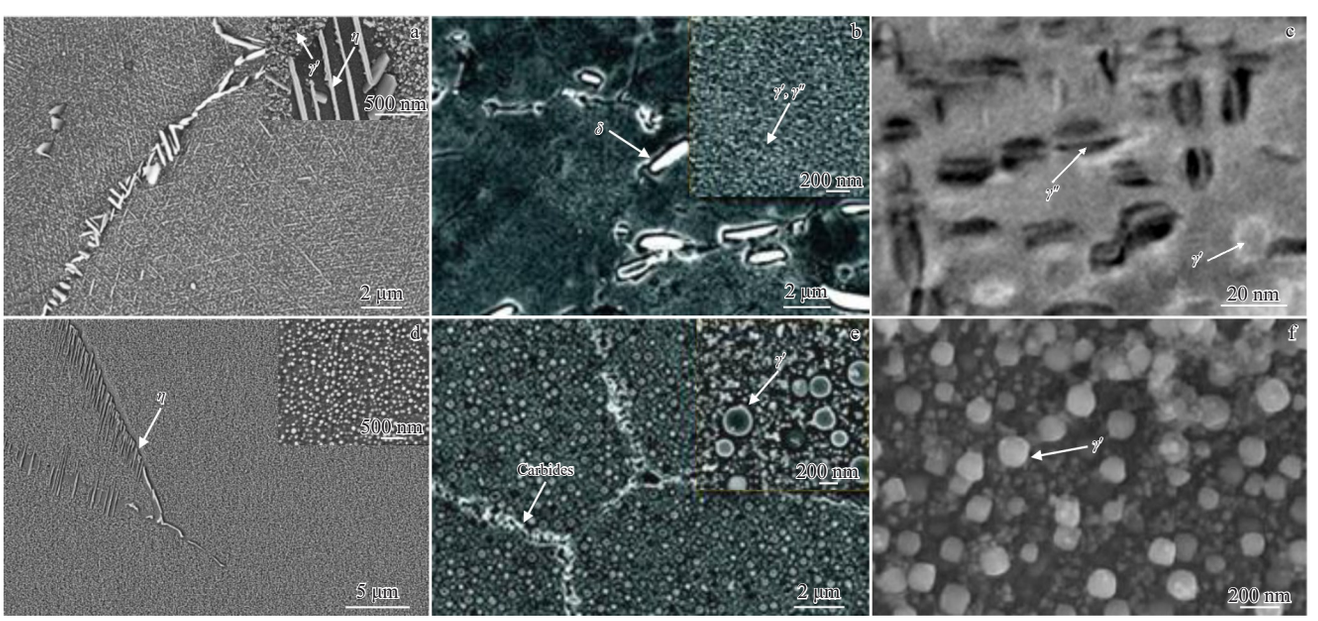

Fig.1 Typical microstructures of Ni-based wrought superalloys[14–15,28–30]: (a) GH4350; (b – c) alloy 718; (d) alloy 718 Plus; (e) Waspaloy; (f) GH4698

Table 1 Chemical composition of typical Ni-based wrought superalloys for fasteners (wt%)[22,32–34]

	Cr	Co	Mo	W	Nb	Al	Ti	Fe	C	P+B	Ta	Ni
Alloy 718	19.0	-	3.0	-	5.15	0.60	0.90	18.5	0.04	0.010	-	Bal.
Alloy 718 Plus	18.0	9.1	2.7	1.0	5.40	1.45	0.75	9.5	0.020	0.011	-	Bal.
Waspaloy	19.0	13.5	4.0	-	-	1.90	3.00	-	0.07	0.005	-	Bal.
GH4698	14.68	-	3.05	-	2.09	1.68	2.70	0.47	0.048	-	-	Bal.
GH4350	17.0	25.0	3.0	2.0	1.20	1.00	2.20	-	≤0.025	≤0.025	4	Bal.

temperatures above 650 °C, the γ'' phase is transformed into the less desirable δ phase, which negatively impacts alloy performance. Alloy 718 Plus addresses this issue by increasing Al and Ti contents and adjusting the Al/Ti value[32]. This modification promotes the precipitation of γ' phase, along with a small amount of η or δ phase, and raises the service temperature by 55 °C[6,29,39–40]. Similar to GH4350, the addition of Co and W aims to enhance mechanical properties, thermal stability, and stress rupture properties through solid solution strengthening[29,35].

Increasing the volume fraction of the γ' phase in superalloys like alloy 718 Plus can improve their service temperature. However, good processing characteristics are also crucial in wrought superalloys alongside high temperature performance. As shown in Table 1, Waspaloy, lacking Nb, contains three times more Ti than alloy 718 Plus, totaling about 5wt% Al+Ti, which results in a γ' phase volume fraction of around 30%. And this enables Waspaloy to withstand temperatures up to 750 °C, higher than that of alloy 718 Plus[33,41–43]. But its processing properties are less favorable compared to alloy 718 Plus due to the higher volume fraction of γ' phase and faster γ' phase precipitation[32]. A similar issue is likely present in GH4698, which has about 4.5wt% Al+Ti. Although its significant γ' phase volume fraction can improve service temperature, it may also face challenges in processing characteristics. The relatively lower Al+Ti content in GH4350 compared to other alloys listed in Table 1 may be intended to moderate γ' phase formation, preventing an excessive increase in deformation resistance, and thus allowing GH4350 to maintain a favorable combination of strength and deformability.

2.1.1 Solid solution strengthening elements

The Ni-based γ phase of the matrix characterized by a fcc crystal structure can dissolve some alloying elements primarily including Co, Cr, Mo, and W. These solute elements interact with matrix and cause lattice misfit and modulus misfit, which will impede dislocation movement and enhance the performance of superalloys[44–45].

The solid solution strengthening effect of each element i ($\Delta\sigma_{SSSi}$) has been quantitatively evaluated in Ni-X_i binary alloy systems by many researchers and they believe that the solid solution strengthening effect results from the interaction of solute atoms with dislocations[45–52]. On this basis, $\Delta\sigma_{SSSi}$ can be calculated by Eq. (1)[53–54]:

$$\Delta\sigma_{SSSi} = K_i c_i^{1/2} \quad (1)$$

where K_i and c_i are strengthening constant and atomic percentage of solute element i, respectively.

In the case of multi-component Ni-based superalloys, the total solid solution strengthening effects ($\Delta\sigma_{SSS}$) can be assessed by the method of Gypen and Deruyttere[55]:

$$\Delta\sigma_{SSS} = \left(\sum_i \Delta\sigma_{SSSi}^{\ 2}\right)^{1/2} \quad (2)$$

Combining Eq. (1) and Eq. (2), the $\Delta\sigma_{SSS}$ is expressed as:

$$\Delta\sigma_{SSS} = \left(\sum_i K_i^{\ 2} c_i\right)^{1/2} \quad (3)$$

K_i can be determined by analyzing 0.2% flow stress experimental data on the solution strengthening of Ni-X_i binary alloys[53–54]. The results are shown in Fig. 2. Elements with larger K_i generally have a greater potential for solid solution strengthening such as Mo, W, Ta, and Nb. It is reasonable for major precipitation strengthening element Al to obtain a low strengthening constant.

The addition of a large amount of Co is one distinguishing feature of GH4350 compared to other Ni-based wrought superalloys. As shown in Fig. 2, adding Co atoms contributes to solid solution strengthening. In addition, as a matrix element, Co facilitates the transformation of part of the γ matrix from fcc to hcp structure, which induces a strengthening effect by the presence of two distinct crystal structures creating a barrier to dislocation motion during cold working[18,56–57]. Another important impact of Co addition is its influence on stacking defects. Co reduces stacking fault (SF) energy, which inhibits the cross-slip motion of dislocations, thereby suppressing dislocation annihilation and improving the ability of twinning, leading to enhanced strain hardening capability of the superalloys[58].

In addition, solid solution strengthening elements are effective only if they successfully enter the matrix. Therefore, these elements must be preferentially partitioned into the γ

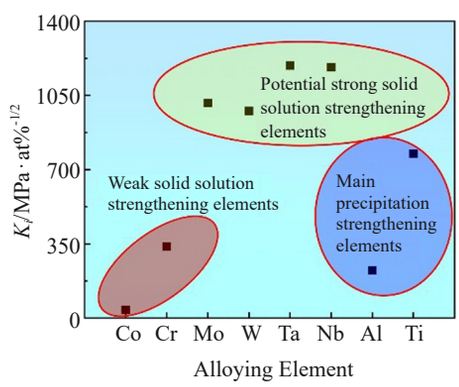

Fig.2 Strengthening constants for solid solution strengthening in Ni[51]

matrix. Alloying elements can be categorized into two groups based on their partitioning coefficient $k_i^{\gamma'}$, as follows[59]:

$$k_i^{\gamma'} = \frac{c_i^{\gamma'}}{c_i^{\gamma}} \tag{4}$$

where $c_i^{\gamma'}$ and c_i^{γ} represent the atomic fractions of element i in the γ' and γ phases, respectively. Elements such as Co, Cr, Mo, and W are typically enriched in the γ phase (with k<1), whereas elements like Al, Ti, and Ta tend to be enriched in the γ' phase (with k>1)[59–60].

Besides, these solid solution strengthening elements must form a stable solid solution in the γ matrix, which can continuously hinder dislocation movement. To maintain their strengthening effect, especially at high temperatures, these elements should not diffuse extensively. This requires a low diffusion rate in the matrix. The diffusion coefficient of element i in the γ phase at temperature T, denoted as $D_T^{i,\mathrm{Ni}}$, is given as follows[61–66]:

$$D_T^{i,\mathrm{Ni}} = D_0^{i,\mathrm{Ni}} \exp\left(\frac{-Q^{i,\mathrm{Ni}}}{RT}\right) \tag{5}$$

where $D_0^{i,\mathrm{Ni}}$ and $Q^{i,\mathrm{Ni}}$ are the pre-exponential factor and the activation energy for interdiffusion of element i in Ni, respectively; R is gas constant.

For example, during the calculation of diffusion coefficients of the elements at 800 °C, the results in Table 2 demonstrate that the diffusion coefficients vary significantly among the elements. Specifically, the diffusion coefficients of Nb, Ta, Ti, and Al are higher, while those of Cr, Co, Mo, and W are lower. As a result, the latter elements diffuse more slowly at high temperatures, thereby better maintaining the solid solution strengthening effect.

In addition to the incorporation of Co, the GH4350 alloy also contains W and Mo, with a combined total mass fraction of 5%. Both W and Mo have relatively high solid solution strengthening constants, indicating their significant contribution to the solid solution strengthening of the alloy[67]. These elements are primarily distributed within the γ matrix phase, and their diffusion coefficients at high temperatures are relatively low, which minimizes their tendency to diffuse out of the matrix. As a result, they effectively maintain the solid solution strengthening effect, thereby significantly enhancing the strength of alloy at elevated temperatures.

Table 2 Diffusion coefficients of typical elements at T= 800 °C[61–62,65–66]

Element	$D_0^{i,\mathrm{Ni}}$/×10^{-5} m^2·s^{-1}	$Q^{i,\mathrm{Ni}}$/kJ·mol^{-1}	$D_{T=800\,^\circ\mathrm{C}}^{i,\mathrm{Ni}}$/×10^{-18} m^2·s^{-1}
Cr	52.0	289	4.45
Co	18.0	282	3.38
Mo	11.5	281	2.41
W	0.86	264	1.21
Nb	8.8	257	27.2
Ta	2.0	251	12.1
Ti	41.0	275	16.9
Al	43.0	272	24.8

2.1.2 Precipitation strengthening elements

Al, Ti, and Nb are typical γ' phase-forming elements, and γ' phase remains stable at high temperatures, effectively hindering dislocation motion. An increase in Al, Ti and Nb content increases the γ' phase volume fraction, which further enhances the strength of alloy. The total mass fraction of Al, Ti, and Nb in GH4350 is 4.5wt%, which signifies a significant potential for precipitation strengthening within the alloy.

In addition to Al, Ti, and Nb, Ta also plays a vital role in strengthening the γ' phase and represents a notable difference in the composition of GH4350 compared to other Ni-based wrought superalloys. Ta is not commonly found in Ni-based wrought superalloys, but is frequently used in Ni-based single crystal superalloys. This discrepancy arises because excessive γ'-phase-forming elements can increase the deformation resistance in Ni-based wrought superalloys, thereby diminishing their cold or hot workability[68]. Conversely, Ni-based single crystal superalloys are cast directly without undergoing cold or hot working processes, allowing for the inclusion of higher amount of γ'-phase-forming element.

The Ta content can vary from 3wt% to 12wt%, and the total amount of main γ'-phase-forming element (Al+Ti+Ta) could exceed 20wt%[69–70]. As a result, the volume fraction of γ' phase of Ni-based single crystal superalloys can surpass 60wt%[71–74]. Researchers have shown that Ta inhibits the coalescence of the γ' phase during isothermal long-term aging, thereby improving the microstructure stability of the γ' phase and increasing its volume fraction[74–78]. Additionally, Ta can enhance oxidation and thermal corrosion resistance of superalloys in certain conditions[79–80].

The addition of Al, Ti, Nb, and Ta in GH4350 actively contributes to maintaining the structural integrity and stability of the γ' phase, effectively inhibiting its dissolution or structural alterations at elevated temperatures. Consequently, the γ' phase continues to impede dislocation motion at high temperatures, thereby strengthening the alloy. This enhancement in γ' phase stability is pivotal for ensuring that the alloy retains its desired properties.

2.2 Precipitation phases of GH4350

Many studies have demonstrated that the precipitation phases of GH4350 are γ' phase and η phase[12–15,20–22,28,56,68,81–84]. The crystal structure of η phase is shown in Fig. 3a. Apparently, the stacking sequence is ABACABAC⋯, which is a typical kind of hcp crystal structure. Fig. 3b and 3c show transmission electron microscope (TEM) image and the chemical composition of γ' phase and η phase in alloy K4750, respectively. The energy dispersive spectrometer (EDS) results show that the η phase is primarily composed of Ni, Al, Ti, and Nb, which is close to the chemical composition of γ' phase.

2.3 Heat treatment of GH4350

2.3.1 Homogenization of as-cast GH4350

Due to the high degree of alloying, wrought superalloys often experience severe dendritic segregation during solidification, leading to poor hot workability[85]. To eliminate

the segregation, an appropriate homogenization heat treatment process is essential and the first step to obtain the target microstructure[85–87]. In the as-cast GH4350 prepared by VIM+VAR, significant elemental segregation occurs with Nb, Ti, and Ta elements enriched in the interdendrites, and Cr, Mo, and Al elements enriched in the dendrites[11]. This segregation is accompanied by the precipitation of Laves phases and acicular phases in the interdendrites, while dispersed γ' phases are also precipitated during the cooling process[11]. To mitigate these issues, a homogenization heat treatment at 1180 °C for 40 h with furnace cooling has been proposed, successfully eliminating elemental segregation and detrimental phases[11]. Achieving a uniform microstructure with consistent elemental composition requires relatively long heat treatment time, and researches on homogenization heat treatments are rare. Therefore, careful design of the melting and homogenization processes is crucial.

2.3.2 Solid solution heat treatment of GH4350

Precipitation phases can be detrimental if they form excessively during solidification, as they can act as sources of cracks. However, these phases are also crucial for precipitation strengthening. Therefore, a comprehensive understanding of the control of precipitation phases in GH4350 is essential. Scanning electron microscope (SEM) images of samples after solid solution treatment at various temperatures for 1 h are shown in Fig.4. The γ' phases begin to dissolve at 1010 ℃, which aligns well with the solvus temperature of γ' phases reported in Ref. [12,81].

As indicated in Fig.4, the η phase is significantly reduced at 1055 ℃. When the temperature rises to 1080 ℃, only sporadic η phase can be observed, and it is completely dissolved at 1095 ℃.

If the alloy is solid-solution-treated below the solvus temperature of the η phase, such as 1050 ℃, the precipitation of the η phase at grain boundaries may be used to control grain size like δ phase[20,88]. As the temperature increases from 800 ℃ to 1070 ℃, the recrystallized grain size increases slightly from approximately 10 μm to 14 μm, while further increasing temperature from 1080 ℃ to 1095 ℃, the grain size increases significantly, approaching 100 μm, due to the lack of η phase pinning at the grain boundaries[82]. Most reported solid-solution temperatures of GH4350 are above the solvus temperature of the η phase[12–13,15,21,68,89]. It appears that controlling grain size with the η phase is not the primary focus of the solid-solution treatment, but the complete dissolution of η phase into the matrix is the ultimate goal. This approach may help to prevent the continuous growth of the η phase during solid solution heat treatment[22].

2.3.3 Aging treatment of GH4350

Aging treatments are performed after solid solution to optimize the precipitations of γ' and η phases[90]. The lower temperature limit of γ' phase precipitation is between 650 and 700 ℃ based on variation in hardness over aging time and temperature (Fig. 5a) for solid-solution-treated GH4350 alloy[12,81].

During aging treatment at 788 ℃, the η phase is observed at the grain boundaries (Fig. 5b, point C_1), indicating that the lower temperature limit for η phase precipitation is approximately 788 °C. When the aging temperature further increases to 816 ℃, maximum hardness is achieved at both solid solution temperatures. At point D_1 in Fig.5b, both γ' and η phases are present.

As indicated in Fig.5c–5f, the growth and morphologies of the η phase vary with heat treatments. Initially, the plate-like η phase precipitates at the grain boundaries (Fig. 5c–5d). With increasing the aging temperature and time, the η phase progressively grows from the grain boundaries to the grains, forming a Widmanstätten morphology structure (Fig.5e–5f).

In conclusion, the precipitation and distribution characteristics of the η phase are significantly affected by the aging heat treatment. A comprehensive understanding of the effect of heat treatment on γ' and η phases precipitation is required to develop a rational heat treatment strategy.

2.4 Phase transformation behavior

From the perspective of phase stability, the η phase is more stable at temperatures of 650 °C or above, which is confirmed by thermodynamic calculations of the phase stability of Nimonic 263 that show the γ' phase is stable up to 750 ℃, while η phase is stable up to 957 ℃[91]. Long-term thermal exposure further supports this point, as the η phase

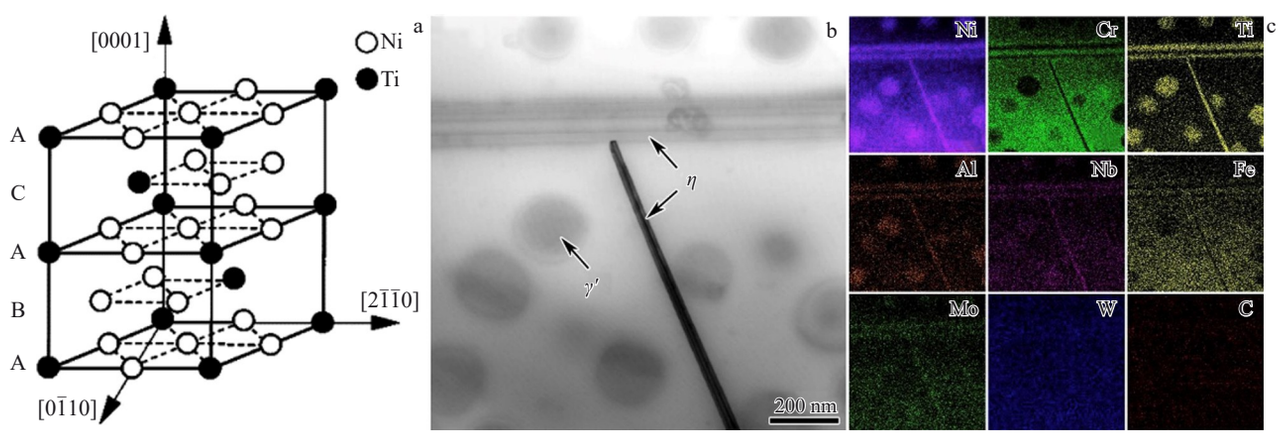

Fig.3 Crystal structure of η phase (a)[83]; TEM image (b) and corresponding EDS mappings (c) of γ' and η phases in alloy K4750[84]

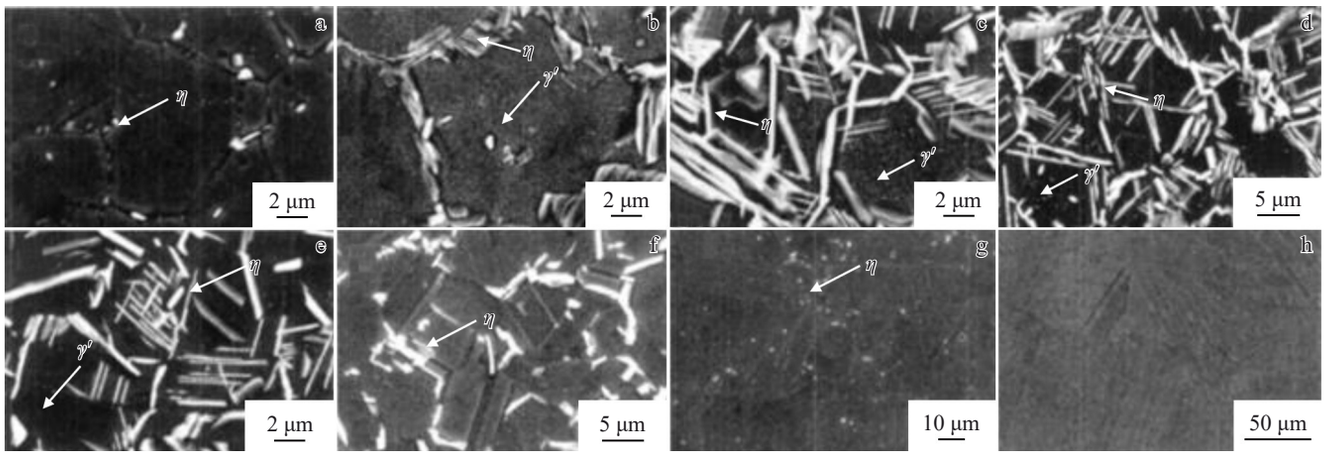

Fig.4 SEM images of samples solid-solution-treated at different temperatures for 1 h[82]: (a) 830 ℃; (b) 950 ℃; (c) 980 ℃; (d) 1010 ℃; (e) 1020 ℃; (f) 1055 ℃; (g) 1080 ℃; (h) 1095 ℃

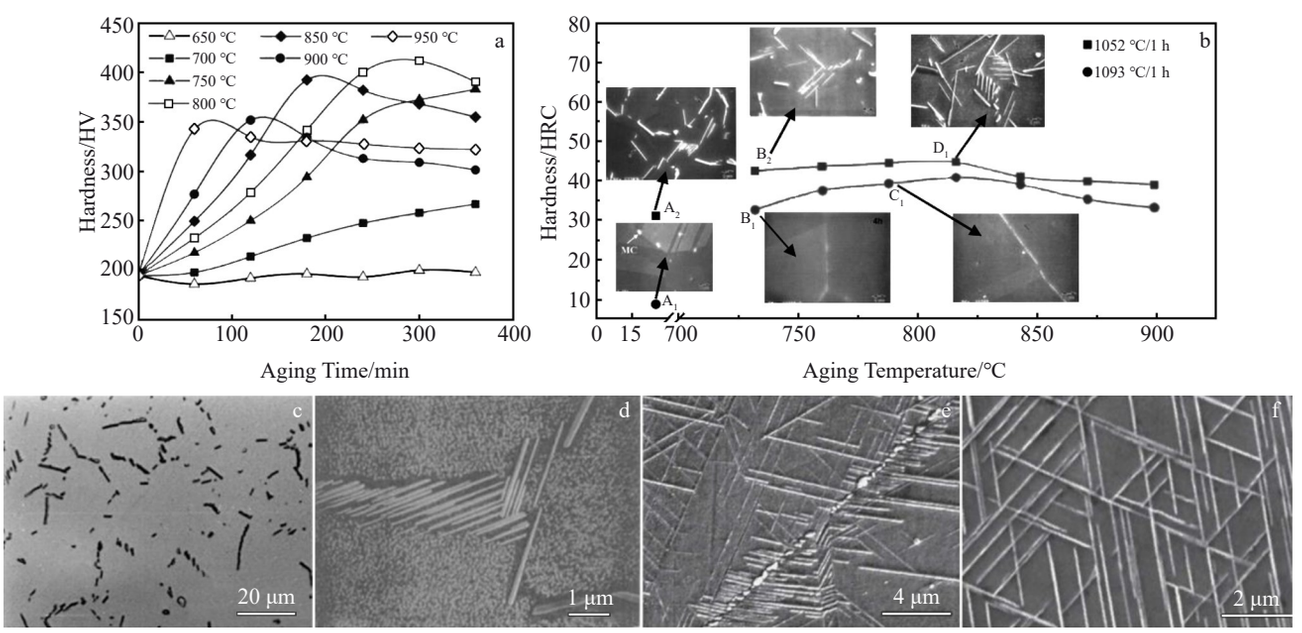

Fig.5 Variation of hardness with aging time for GH4350 solid-solution-treated at various temperatures (a); variation of hardness with aging temperature for solid-solution-treated GH4350 and corresponding microstructures for several typical points (b)[12]; morphologies of η phase after solid-solution treatment at approximately 1050 ℃ for 1 h followed by aging-treatment at 750 ℃ for 1 h (c) and at 899 ℃ for 4 h+816 ℃ for 4 h (d)[22]; grain boundary area (e) and grain interior (f) of η phase after solid-solution treatment at 1100 ℃ for 1 h+aging at 1000 ℃ for 3 h[81]

predominates throughout the matrix, and nearly all γ' particles dissolve when the alloy is exposed at 870 °C for 8000 h[92].

The chemical composition of the γ' and η phases is similar to their primary distinctions being their crystal structures. The γ' to η transformation occurs through the introduction of SFs into the γ' phase formed by the systematic passage of Shockley partials[68,84,91–96]. As shown in Fig. 6, theoretically, if the A layer is added by the introduction of extrinsic SFs in γ' between B layer and C layer, the stacking sequence will become ABACABAC..., which is actually identical to the stacking sequence along the close packed planes (0001) in η phase. Experimental observation, as shown in Fig. 7a – 7d, indicates that the η phase grows at the expense of γ' phase, with γ' precipitation-free zones (PFZs) forming around each η phase. The above information suggests a close relationship among η phase formation, the γ' phase, and SFs.

Additionally, Fig. 7e – 7h demonstrate that SFs, induced by numerous paired dislocations, appear to elongate and eventually transform into the growing η phase at the expense of γ' phase.

More precise evidence in experiment indicates that two-layer extrinsic faults found in γ' phase (Fig. 8a and 8b) are formed by the passage of two identical 1/6<112> Shockley partials on consecutive {111} planes, and η phase forming

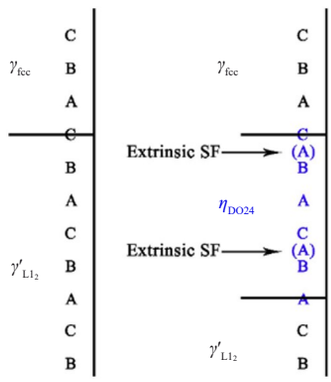

Fig.6 Illustration of γ' to η transformation by introduction of extrinsic SFs

elements, such as Ta, Nb, and Ti, are segregated along superlattice extrinsic stacking faults (SESFs) confirmed by high spatial resolution EDS mappings (Fig.8c).

These images indicate that SFs in the γ' phase may serve as local nucleation sites for the η phase. Fig.9a and 9b show that the nucleation and growth of η phase have two paths, where η phase directly precipitates within extra-large γ' (EL-γ') when the coalescence of γ' phases reaches a critical stage, and η phase precipitates at the interface between small *M*C carbides and EL-γ' with both *M*C carbides and η embedded within EL-γ'[43].

Interestingly, as shown in Fig. 9c – 9d, both paths share a common feature that they both lead to the formation of SFs. Notably, *M*C carbides are segregated with Ti and the nucleation and growth of η phase in the second path (with *M*C-II carbide) occur more rapidly than in the first path (without carbide)[40]. This suggests that *M*C-II carbide is a more effective provider of η phase-forming elements compared to EL-γ' in this study.

Based on the preceding discussion, two criteria for the formation and growth of the η phase can be concluded: (1) SFs initially serve as nucleation sites; (2) sufficient η phase-forming elements must be present during nucleation and growth. To better regulate the microstructure and the properties of superalloys, further research into the mechanisms of η phase nucleation and growth is necessary. This will enhance our understanding and control over η phase development.

3 Roles of η Phase

To address the need for higher operating temperatures in fasteners, increasing the number of γ' phase strengthening elements may enhance the high-temperature performance. However, at temperatures above 650 °C, the γ' to η phase transformation occurs, leading to a decrease in γ' phase volume fraction and consequently reducing its strengthening effect. Therefore, understanding the impact of the η phase on the properties of superalloys is crucial.

As previously discussed, the η phase initially precipitates at the grain boundaries (intergranular) and evolves into a Widmanstätten morphology with the increase in time and temperature (intragranular). Researchers have identified four distinct forms of the η phase, i. e. needle-like, plate-like, granular, and short rod-like (Fig. 10), each of which impacts the properties of superalloys differently[23,95].

This characteristic affects the morphology of grain boundaries, significantly impacting strengthening effect. It is reported that the discontinuous precipitation of plate-like η phase exerts a pinning effect on the grain boundary, leading to the formation of grain boundary serrations, whose magnitude is increased with the increase in inclination angle with respect to the grain boundaries[6,29,95]. Grain boundary serrations and intergranular and intragranular η phase influence the properties of superalloys.

3.1 Effects of η phase on crack initiation and propagation

Serrated grain boundaries induced by η phase can enhance the creep resistance by reducing cavitation and crack propagation rates, and they also appear to retard the propagation of intergranular cracks to some extent during

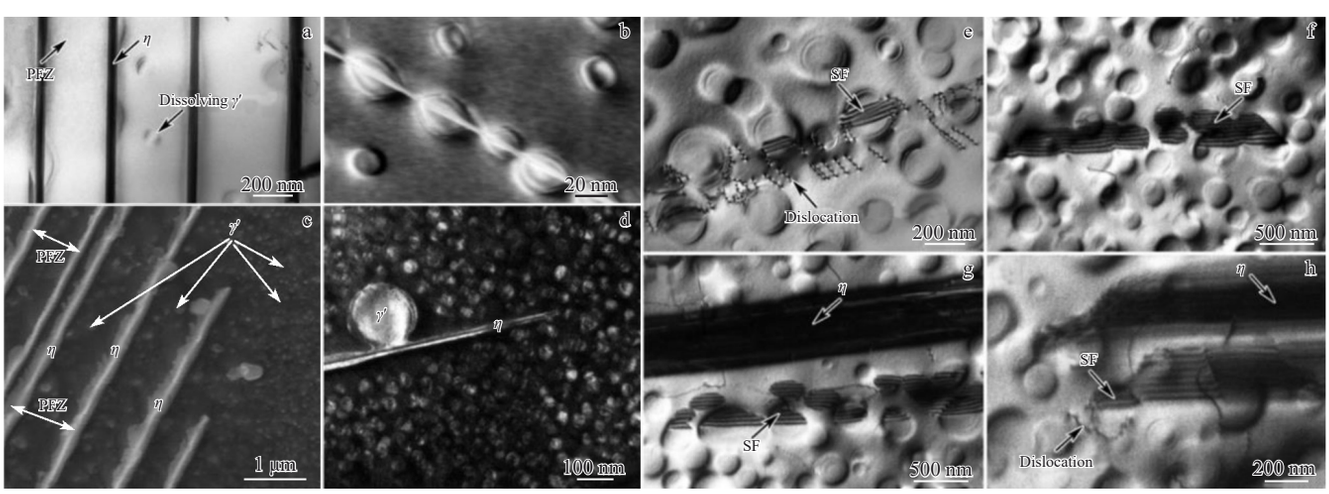

Fig.7 Typical micrographs of η phase growth by consuming γ' phase of various superalloys[68,87,95–96]: (a) K4750; (b) GH4350; (c) A286; (d) alloy 718 plus; TEM images of SFs and η phase in K4750 (e–h)

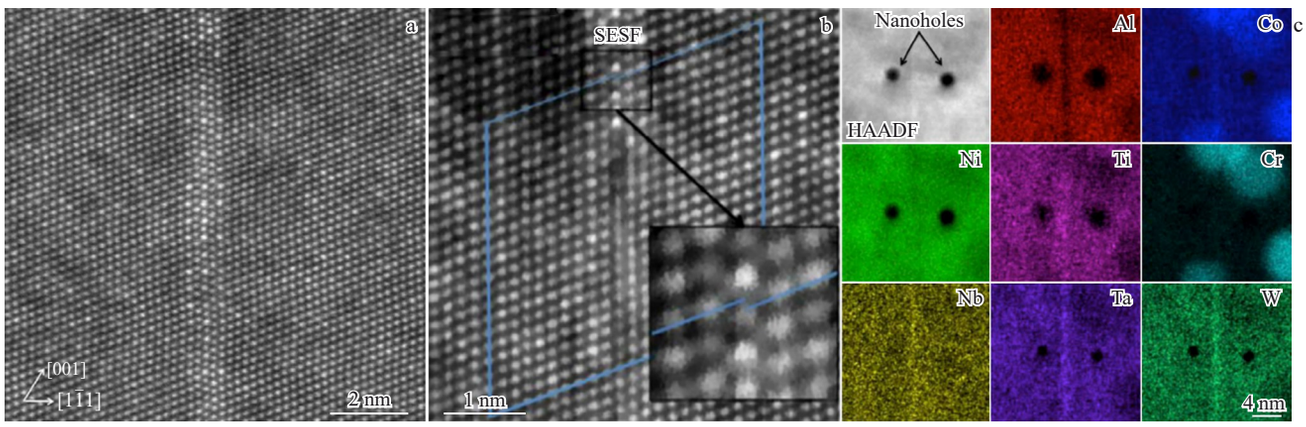

Fig.8 More precise evidence of γ' to η phase transformation in experiment[93]: (a) high angle angular dark field-scanning transmission electron microscope (HAADF-STEM) image of a grid-like ordering along a SESF inside a γ' precipitate; (b) Shockley partials at leading SESF showing by Burgers circuit analysis; (c) EDS element mappings of a vertical SESF showing segregation along the fault

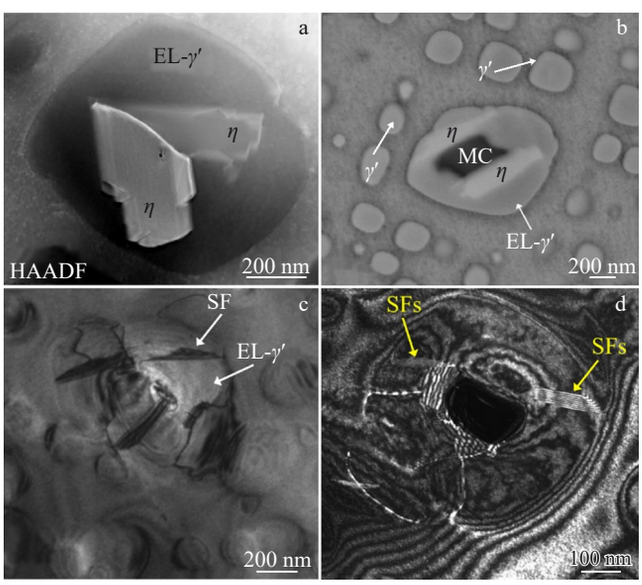

Fig.9 Two paths of formation of η phase and SFs[43]: (a, c) direct precipitation within EL-γ'; (b, d) precipitation at interface of small size *M*C carbides and EL-γ'

fatigue test[25–26]. This suggests a potential beneficial effect of the η phase-induced serrated grain boundaries in impeding crack propagation along grain boundaries.

Additionally, small η phases at grain boundaries typically do not initiate cavities during creep though dislocations piled up ahead of them[84]. Fig. 11a shows two grain boundary cavities whose growth appears to be constrained by impingement on η phase platelet. 2%–3% (area fraction) η phase, which extended from grain boundaries across the PFZs, may be beneficial to creep strength and ductility by constraining grain boundary cavity growth[24]. These findings collectively indicate that the η phases whether in small sizes at grain boundaries or within a restricted area may not necessarily have a detrimental effect on creep properties. Instead, in certain configurations, they may exhibit a neutral or even a beneficial role in enhancing creep strength and ductility by impeding cavity growth along grain boundaries.

However, Fig. 11b – 11c present backscattered electron micrographs of STAL15-CC alloy after creep at 850 ℃, showing secondary cracks forming around η layers at grain boundaries. Cracks tend to form around the η phases, indicating that intergranular η phases may act as brittle sites at the grain boundaries, thus serving as sites for crack initiation during creep tests[27]. During the fatigue processes, stress concentration as a result of dislocations accumulation and networks formation at the edges of η precipitates can induce

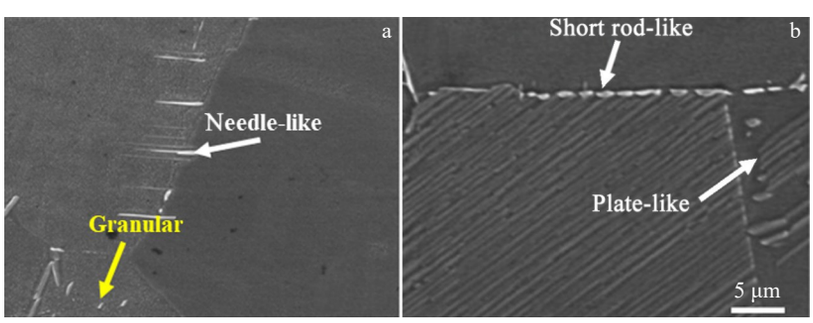

Fig.10 Morphologies of needle-like+granular (a) and plate-like+short rod-like (b) η phases[23]

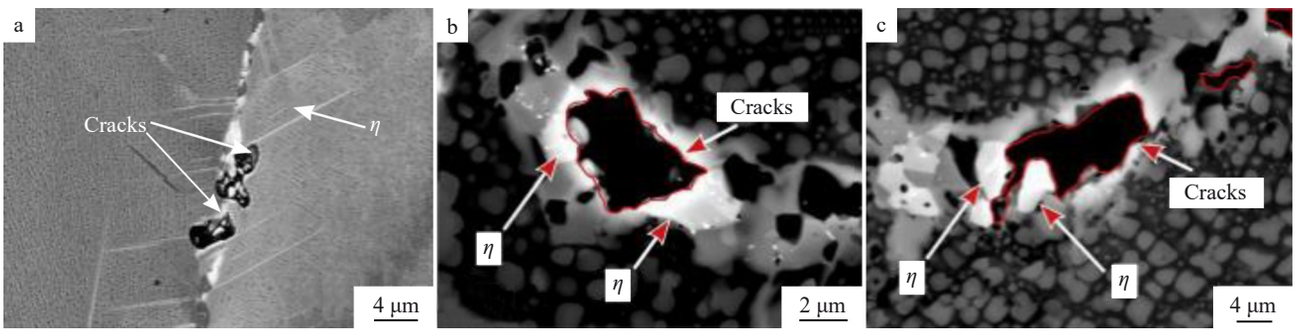

Fig.11 Two grain boundary cavities (a)[24]; backscattered electron micrographs of STAL15-CC alloy after creep at 850 °C (b–c)[27]

the initiation and propagation of microcracks[25]. These results suggest that the impact of η phases on crack initiation and propagation varies depending on specific conditions, such as loading type (creep or fatigue) and microstructural characteristics, underscoring the complexity and multifaceted nature of the η phase in superalloys.

Understanding the circumstances under which the η phase acts as a crack initiation site or stress concentrator when η phase potentially impedes crack propagation is crucial. This understanding will greatly aid in optimizing superalloy designs for harness-beneficial effects or to mitigate detrimental influences of the η phase on properties.

3.2 Effects of η phase on dislocation hindrance

As a precipitation phase, η phase is expected to contribute to precipitation strengthening similar to the γ' phase. For instance, with the prolongation of aging time from 25 h to 100 h, the ultimate tensile strength (UTS) of alloy 718 Plus significantly improves from 797 MPa to 860 MPa with an increase in volume fraction of plate-like/needle-like η phases[23]. Notably, during this period, the volume fraction of γ' phase decreases from approximately 32% to 28%[23]. This suggests that the strengthening effect of the γ' phase is comparatively weaker. Consequently, the observed enhancement in tensile properties is attributed to the precipitation of a significant number of plate-like and needle-like η phases. TEM image further confirm that the improved UTS is due to the hindrance of dislocation motion at grain boundaries and within grains near the η phases (Fig. 12a and 12c).

The effect of η phase on dislocation hindrance is also reported in a research of stress relaxation behavior of GH4350, it is concluded that the enhanced stress relaxation resistance at 800 °C is attributed to the dislocation blocking by η phases, as shown in Fig.12d[15]. This study also compares the stress relaxation resistance of Waspaloy and GH4350 at various temperatures. At 600 °C, dislocations are still impeded by intragranular η phases (Fig. 12b). However, the larger size and higher mass fraction of γ' phases in Waspaloy are key factors in hindering the movement of dislocations. While the number of intragranular η phases in GH4350 is rather small, thus η phases contribute slightly to the relaxation resistance at

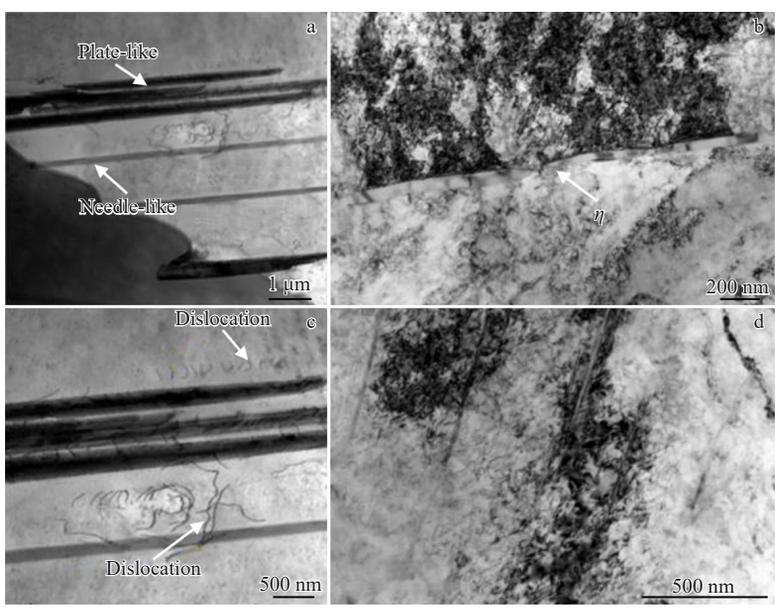

Fig.12 Bright-field TEM images of η phases and dislocations[15,23]: (a, c) grain boundary η phases and dislocations in grain, (b) microstructures of GH4350 after relaxation at 600 °C, and (d) microstructures of GH4350 after relaxation at 800 °C

this temperature, leading a better stress relaxation resistance of Waspaloy than that of GH4350[15].

4 Conclusions

1) GH4350 incorporates significant amounts of Co, Mo, and W to enhance solid solution strengthening, as quantified through modeling, and it maintains a moderate Al+Ti+Nb content to balance it precipitation strengthening with deformability. The addition of Ta not only stabilizes the γ' phase and increases its volume fraction, but also improves oxidation and thermal corrosion resistance.

2) The primary precipitation phases in GH4350 are γ' and η, which can be controlled through heat treatment under various temperatures and durations. A homogenization heat treatment at 1180 °C for 40 h with furnace cooling effectively removes elemental segregation and undesirable phases, providing a foundation for subsequent phase control.

3) The lower temperature limit for γ' phase precipitation is between 650 and 700 °C, with a solvus temperature around 1010 °C. For η phase, precipitation begins at approximately 788 °C. As temperature and time increase, η phase precipitates from grain boundaries into the grains, developing a Widmanstätten morphology, and eventually dissolves completely at temperatures nearing 1095 °C. Solid solution heat treatment below this temperature may be able to control grain size through the undissolved η phase.

4) The γ' to η phase transformation occurs because η phase is more stable above 650 °C. Both phases share similar elemental composition and transformable crystal structures, which is caused by the introduction of SFs. This transformation is accelerated due to the presence of effective η phase-forming elements providers, such as *M*C-type carbides, surrounding the γ' phase.

5) Small quantities of η phase with needle-like, plate-like, granular, and short rod-like morphologies can improve properties such as creep resistance, tensile strength, fatigue resistance, and stress relaxation resistance by reducing cavitation, decreasing crack propagation, and hindering dislocation movement. Conversely, a large volume of η phase with Widmanstätten morphology can negatively impact mechanical properties, as the brittleness of η phase and associated stress concentrations lead to crack initiation and growth, ultimately depleting γ' phase and diminishing its strengthening effect.

References

1 Pan Y, Wen M. *Vacuum*[J], 2018, 156: 419

2 Pan Y, Pu D L, Li Y Q *et al*. *Materials Science and Engineering B*[J], 2020, 259: 114580

3 Pan Y, Yang F H. *Journal of Materials Research and Technology*[J], 2024, 28: 381

4 Pan Y. *Vacuum*[J], 2017, 143: 165

5 Liang L, Xu M F, Chen Y H *et al*. *Materials Science and Engineering A*[J], 2021, 819: 141507

6 Pickering E J, Mathur H, Bhowmik A *et al*. *Acta Materialia*[J], 2012, 60(6–7): 2757

7 Chen T W, Wang P T, Kang Y C *et al*. *Journal of Alloys and Compounds*[J], 2023, 960: 170620

8 Fecht H, Furrer D. *Advanced Engineering Materials*[J], 2000, 2(12): 777

9 Pan Y. *Journal of Materials Research and Technology*[J], 2023, 26: 8813

10 Melhem G N. *Encyclopedia of Aluminum and Its Alloys*[M]. Boca Raton: CRC Press, 2018

11 Li Kemin, Yang Yujun, Wang Zhigang *et al*. *Journal of Iron and Steel Research International*[J], 2012, 24(7): 54

12 Asgari S. *Metallurgical and Materials Transactions A*[J], 2006, 37(7): 2051

13 Najafi H, Asgari S. *Materials Science and Engineering A*[J], 2005, 398(1–2): 204

14 Jiang H, Yang J, Dong J X *et al*. *Proceedings of the 9th International Symposium on Superalloy 718 & Derivatives: Energy, Aerospace, and Industrial Applications*[C]. Cham: Springer International Publishing, 2018: 789

15 Wang Y Z, Dong J X, Zhang M C *et al*. *Materials Science and Engineering A*[J], 2016, 678: 10

16 Jiang He, Dong Jianxin, Zhang Maicang *et al*. *Acta Metallurgica Sinica*[J], 2019, 55(9): 1211 (in Chinese)

17 Ferrero J G. *Journal of Materials Engineering and Performance*[J], 2005, 14(6): 691

18 SPS TECHNOLOGY. *Superalloys Developed by SPS Technologies for Aerospace Fasteners*[EB/OL]. https://www.pccfasteners.com/assets/local/documents/product-literature/superalloy_brochure.pdf

19 Du Jinhui, Lv Xudong, Dong Jianxin *et al*. *Acta Metallurgica Sinica*[J], 2019, 55(9): 1115 (in Chinese)

20 Samiee M, Asgari S. *Scripta Materialia*[J], 2007, 57(2): 93

21 Farvizi M, Asgari S. *Materials Science and Engineering A*[J], 2008, 480(1–2): 434

22 Kermajani M. *Materials Science and Engineering A*[J], 2012, 534: 547

23 Li J, Wu Y T, Liu Y C *et al*. *Materials Characterization*[J], 2020, 169: 110547

24 Shingledecker J P, Pharr G M. *Metallurgical and Materials Transactions A*[J], 2012, 43(6): 1902

25 Qi Q Q, Zhang H J, Liu C X *et al*. *Materials Science and Engineering A*[J], 2020, 798: 140132

26 Hong H U, Kim I S, Choi B G *et al*. *Materials Science and Engineering A*[J], 2009, 517(1): 125

27 Kontis P, Kostka A, Raabe D. *Acta Materialia*[J], 2019, 166: 158

28 Asgari S. *Journal of Materials Processing Technology*[J], 2001, 118(1–3): 246

29 Alabbad B, Tin S. *Materials Characterization*[J], 2019, 151: 53

30 Zhao Yihan, Peng Jianqiang, Zhang Xiaowu *et al*. *Heat Treatment of Metals*[J], 2016, 41(8): 56 (in Chinese)

31 Devaux A, Nazé L, Molins R *et al*. *Materials Science and*

Engineering A[J], 2008, 486(1–2): 117

32 Hosseini E, Popovich V A. *Additive Manufacturing*[J], 2019, 30: 100877

33 Slama C, Abdellaoui M. *Journal of Alloys and Compounds*[J], 2000, 306(1–2): 277

34 Zhang M, Ma C C, Chun X *et al. Rare Metal Materials and Engineering*[J], 2024, 53(8): 2131

35 Kennedy R L. *International Symposinm on Superalloys 718, 625, 706 and Various Derivatives* (*2005*)[C]. Warrendale: TMS, 2005: 1

36 Hassan B, Corney J. *Materials Science and Technology*[J], 2017, 33(16): 1879

37 Kienl C, Mandal P, Lalvani H *et al*. *Metallurgical and Materials Transactions A*[J], 2020, 51(8): 4008

38 Göken M, Kempf M. *Acta Materialia*[J], 1999, 47(3): 1043

39 Kinzel S, Gabel J, Völkl R *et al*. *Advanced Engineering Materials*[J], 2015, 17(8): 1106

40 Liu G, Xiao X S, Véron M *et al*. *Acta Materialia*[J], 2020, 185: 493

41 Agnoli A, Le Gall C, Thebault J *et al*. *Metallurgical and Materials Transactions A*[J], 2018, 49(9): 4290

42 Wang M X, Zhu H, Yang G J *et al. Materials & Design*[J], 2021, 198: 109359

43 Kou H B, Li W G, Ma J Z *et al*. *International Journal of Mechanical Sciences*[J], 2018, 140: 83

44 Butt M Z. *Philosophical Magazine Letters*[J], 1989, 60(4): 141

45 Gypen L A, Deruyttere A. *Scripta Metallurgica*[J], 1981, 15(8): 815

46 Kratochvíl P, Lukáč P, Sprušil B. *Czechoslovak Journal of Physics*[J], 1973, 23(6): 621

47 Labusch R. *Physica Status Solidi* (*b*)[J], 1970, 41(2): 659

48 Fleisgher R L. *Acta Metallurgica*[J], 1961, 9(11): 996

49 Fleischer R L. *Acta Metallurgica*[J], 1963, 11(3): 203

50 Mishima Y, Ochiai S, Hamao N *et al*. *Transactions of the Japan Institute of Metals*[J], 1986, 27(9): 648

51 Roth H A, Davis C L, Thomson R C. *Metallurgical and Materials Transactions A*[J], 1997, 28(6): 1329

52 Mishima Y, Ochiai S, Hamao N *et al*. *Transactions of the Japan Institute of Metals*[J], 1986, 27(9): 656

53 Gypen L A, Deruyttere A. *Journal of Materials Science*[J], 1977, 12(5): 1034

54 Chen Y T, Yeh A C, Li M Y *et al*. *Materials & Design*[J], 2017, 119: 235

55 Chen X M, Ning M T, Hu H W *et al*. *Materials Characterization*[J], 2023, 201: 112916

56 Hosseinifar M, Asgari S. *Materials Science and Engineering A*[J], 2010, 527(27): 7313

57 Li Kemin, Han Guangwei, Deng Bo. *Acta Aeronautica et Astronautica Sinica*[J], 2012, 33(6): 1156 (in Chinese)

58 Yang C L, Zhang Z J, Zhang P *et al*. *Materials Science and Engineering A*[J], 2018, 736: 100

59 Giese S, Bezold A, Pröbstle M *et al*. *Metallurgical and Materials Transactions A*[J], 2020, 51(12): 6195

60 Fayman Y C. *Materials Science and Engineering*[J], 1986, 82, 203

61 Karunaratne M S A, Reed R C. *Defect and Diffusion Forum*[J], 2005, 237–240: 420

62 Jung S B, Yamane T, Minamino Y *et al*. *Journal of Materials Science Letters*[J], 1992, 11(20): 1333

63 He C, Liu L, Huang T W *et al*. *Journal of Alloys and Compounds*[J], 2020, 836: 155486

64 Pröbstle M, Neumeier S, Feldner P *et al*. *Materials Science and Engineering A*[J], 2016, 676: 411

65 Karunaratne M S A, Carter P, Reed R C. *Materials Science and Engineering A*[J], 2000, 281(1–2): 229

66 Karunaratne M S A, Carter P, Reed R C. *Acta Materialia*[J], 2001, 49(5): 861

67 Cheng Yuan, Zhao Xinbao, Yue Quanzhao *et al. Rare Metal Materials and Engineering*[J], 2023, 52(7): 2599 (in Chinese)

68 Asgari S, Sharghi-Moshtaghin R, Sadeghahmadi M *et al*. *Philosophical Magazine*[J], 2013, 93(10–12): 1351

69 Xia W S, Zhao X B, Yue L *et al*. *Journal of Materials Science & Technology*[J], 2020, 44: 76

70 Long H B, Mao S C, Liu Y N *et al*. *Journal of Alloys and Compounds*[J], 2018, 743: 203

71 Ali M A, López-Galilea I, Gao S *et al*. *Materialia*[J], 2020, 12: 100692

72 Yang W C, Yue Q Y, Cao K L *et al*. *Materials Characterization*[J], 2018, 137: 127

73 Shui L, Jin T, Tian S G *et al*. *Materials Science and Engineering A*[J], 2007, 454–455: 461

74 Wu J J, Jiang X W, Wang Y *et al*. *Materials Science and Engineering A*[J], 2021, 806: 140829

75 Costa A M S, Oliveira J P, Salgado M V *et al*. *Materials Science and Engineering A*[J], 2018, 730: 66

76 Peng P, Lu L, Liu Z J *et al*. *Journal of Alloys and Compounds*[J], 2022, 920: 165886

77 Xu Yangtao, Wang Tongchao, Lv Xin. *Rare Metal Materials and Engineering*[J], 2023, 52(11): 3939 (in Chinese)

78 Lai Yongjun, Ning Likui, Zhao Ling *et al*. *Rare Metal Materials and Engineering*[J], 2024, 53(3): 748 (in Chinese)

79 Park S J, Seo S M, Yoo Y S *et al*. *Corrosion Science*[J], 2015, 90: 305

80 Han F F, Chang J X, Li H *et al*. *Journal of Alloys and Compounds*[J], 2015, 619: 102

81 Tomasello C M, Pettit F S, Birks N *et al*. *International Symposium on Superalloys*[C], Warrendale: TMS, 1996: 145

82 Wan W J, Han G W, Deng B. *Journal of Iron and Steel Research International*[J], 2010, 17(3): 67

83 Dong Jianxin, Li Linhan, Li Haoyu *et al*. *Acta Metallurgica Sinica*[J], 2015, 51(10): 1207 (in Chinese)

84 Liang X, Zhang R, Yang Y *et al*. *International Symposium on*

Superalloys 718, 625, 706 and Various Derivatives[C]. Warrendale: TMS, 1994: 947

85 Zhang Xianguang, Chen Jiajun, Yang Wenchao *et al*. *Rare Metal Materials and Engineering*[J], 2024, 53(1): 136 (in Chinese)

86 Hagihara K, Nakano T, Umakoshi Y. *Acta Materialia*[J], 2003, 51(9): 2623

87 Hou K L, Ou M Q, Wang M *et al*. *Materials Science and Engineering A*[J], 2019, 763: 138137

88 Yang Zhiming, Chen Zijian, Lin Yongcheng *et al. Rare Metal Materials and Engineering*[J], 2023, 52(9): 3147 (in Chinese)

89 Wan W J, Han G W, Deng B. *Journal of Iron and Steel Research International*[J], 2010, 17(1): 64

90 Wang Guang, Song Wei, Liang Jingjing *et al*. *Rare Metal Materials and Engineering*[J], 2024, 53(3): 787 (in Chinese)

91 Zhao J C, Ravikumar V, Beltran A M. *Metallurgical and Materials Transactions A*[J], 2001, 32(6): 1271

92 Kim I S, Choi B G, Hong H U *et al*. *Materials Science and Engineering A*[J], 2014, 593: 55

93 Smith T M, Esser B D, Antolin N *et al*. *Acta Materialia*[J], 2015, 100: 19

94 Smith T M, Esser B D, Antolin N *et al*. *Nature Communications*[J], 2016, 7(1): 13434

95 Tang L T, Zhang H Y, Guo Q Y *et al*. *Materials Characterization*[J], 2021, 176: 111142

96 Seifollahi M, Razavi S H, Kheirandish S *et al*. *Journal of Materials Engineering and Performance*[J], 2013, 22(10): 3063

镍基变形高温合金GH4350的微观结构特征和强化机制

金巨烽[1,2]，赵新宝[1,3]，赵倩敏[1,2]，岳全召[1]，谷月峰[1,3]，张　泽[1,3]

(1. 浙江大学 材料科学与工程学院 高温合金研究所，浙江 杭州 310027)

(2. 浙江大学 工程师学院，浙江 杭州 310027)

(3. 浙江大学 硅及先进半导体材料全国重点实验室，浙江 杭州 310027)

摘　要：GH4350（AEREX 350）是一种紧固件用镍基变形高温合金，最高使用温度可达750 ℃。GH4350具备高抗拉伸强度的同时，能抗疲劳、抗应力断裂、抗应力松弛和耐腐蚀，并具备低膨胀系数和缺口敏感性。该合金主要通过固溶强化以及γ'相沉淀强化，在γ'相析出的同时也会析出少量η相。研究指出，该合金的微观结构对热处理条件十分敏感，包括温度和时间，γ'相在某些热处理条件下会转变为η相，从而可能降低合金的性能。本文概述了GH4350的元素组成特点、受热处理调控的微观结构特征以及强化机制，旨在理解该合金性能优异的原因，并指导新型合金或性能优化型合金的开发，以进一步提高其承温能力。

关键词：紧固件用变形高温合金GH4350；高温性能；元素组成；热处理；η相

作者简介：金巨烽，男，2000年生，硕士，浙江大学工程师学院，浙江 杭州 310027，电话：0571-64219632，E-mail：jinjufeng@zju.edu.cn